Green Chemistry

Accepted Manuscript

This is an *Accepted Manuscript*, which has been through the Royal Society of Chemistry peer review process and has been accepted for publication.

Accepted Manuscripts are published online shortly after acceptance, before technical editing, formatting and proof reading. Using this free service, authors can make their results available to the community, in citable form, before we publish the edited article. We will replace this *Accepted Manuscript* with the edited and formatted *Advance Article* as soon as it is available.

You can find more information about *Accepted Manuscripts* in the Information for Authors.

Please note that technical editing may introduce minor changes to the text and/or graphics, which may alter content. The journal's standard Terms & Conditions and the Ethical guidelines still apply. In no event shall the Royal Society of Chemistry be held responsible for any errors or omissions in this *Accepted Manuscript* or any consequences arising from the use of any information it contains.

ROYAL SOCIETY OF CHEMISTRY

www.rsc.org/greenchem

Please do not adjust margins

Green Chemistry

ARTICLE

Ru catalysts for levulinic acid hydrogenation with formic acid as a hydrogen source

Received 00th January 20xx,
Accepted 00th January 20xx

DOI: 10.1039/x0xx00000x

www.rsc.org/

Agnieszka M. Ruppert,[a] Marcin Jędrzejczyk,[a] Olga Sneka-Płatek,[a] Nicolas Keller,[b] Alexandre S. Dumon,[c] Carine Michel,[c] Philippe Sautet,[c] Jacek Grams[a]

The catalytic hydrogenation of levulinic acid (LA) with a formic acid (FA) as a hydrogen source into γ-valerolactone (GVL) is considered as one of crucial sustainable processes in today's biorefinery schemes. In current work, we investigated the modification of Ru/C as efficient catalysts for both formic acid decomposition and levulinic acid hydrogenation in comparison to Pd and Pt catalysts. In order to better understand what features are responsible for high catalytic performance, we combine experimental tests, DFT calculations together with extensive material characterization. In LA hydrogenation with FA as hydrogen source, the intermediate surface formate inhibits at least partially the LA hydrogenation. In addition, the FA decomposition is highly sensitive to the kind of the preparation method of the Ru/C catalyst: (i) the process looks structure sensitive favored on larger particles (ii) residual chlorine decreases significantly the FA decomposition rate.

Introduction

Over the last decade, intensive research in the field of biomass valorization has resulted in the selection of a number of products called platform chemicals, which can play pivotal role in future biorefinery schemes. Among them, levulinic acid (LA) issued from the transformation of lignocellulosic biomass, and its hydrogenation product, γ-valerolactone (GVL), attracted a significant attention.[1,2,3,4]

Many noble and transition metal catalysts like Ir, Ru, Ni, Pt, Au, Pd or Cu have been investigated for the production of GVL from LA with external hydrogen,[5,6,7,8] considering also solvent [9,10] and metal-support effects.[9,11,12] Ru is often a metal of choice in a protic solvent as we recently explained by combining experimental and DFT calculation studies.[13] As a consequence, heterogeneous Ru-based catalysts are of high interest in liquid phase (de)-hydrogenation reactions.[14] Progress has been performed in the field by studying the behavior of mono and bimetallic catalytic systems,[15,16] New bimetallic Au-Pd/TiO_2 and Ru-Pd/TiO_2 catalysts with high activity, selectivity towards GVL and with improved stability, were recently reported by the group of Weckhuysen.[1]

For improving further the biomass hydrogenation process, a very interesting alternative approach to hydrogenation by externally supplied hydrogen is transfer hydrogenation. In the case of GVL synthesis, transfer hydrogenation is especially suitable, as the hydrolysis of (ligno)cellulose produces formic acid (FA) in equimolar amounts to LA.[17] In the presence of a selective catalyst, FA decomposes into carbon dioxide and hydrogen, and therefore can be used as an internal hydrogen source in the LA hydrogenation into GVL (Scheme 1).

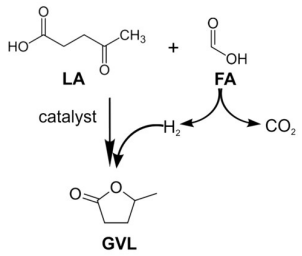

Scheme 1. GVL production from LA with FA as a hydrogen source

Ruthenium-based homogeneous catalysts such as *e.g.* [(η6-C6Me_6)Ru(bpy)(H_2O)][SO_4] or $RuCl_3$/PPh_3, were first proven to be efficient for this reaction.[18,19,20] However, drawbacks such as notably a poor stability and a weak resistance to water or to mineral acids issued from real biomass feedstock hydrolysis, forced consequently scientists to develop more stable heterogeneous catalysts. In this frame, gold-based catalysts were very attractive in the LA hydrogenation with FA as internal hydrogen source.[21,22] By evaluating several oxides and active carbon as support for metallic Au nanoparticles, Du et

[a] Institute of General and Ecological Chemistry, Faculty of Chemistry, Łódź University of Technology, ul. Żeromskiego 116, 90-924 Łódź, Poland. E-mail: agnieszka.ruppert@p.lodz.pl
[b] Institut de Chimie et Procédés pour l'Energie, l'Environnement et la Santé, ICPEES, CNRS, University of Strasbourg, 25 rue Becquerel, 67087, Strasbourg, France.
[c] Université de Lyon, CNRS, Ecole normale supérieure de Lyon, Institut de Chimie de Lyon, Laboratoire de Chimie, 46 allée d'Italie, 69364 Lyon Cedex 07 France.
Electronic Supplementary Information (ESI) available: [details of any supplementary information available should be included here]. See DOI: 10.1039/x0xx00000x

Green Chemistry Accepted Manuscript

al. evidenced the crucial role of the support and highlighted that zirconia was the most promising support, an excellent 99% GVL yield being achieved over Au/ZrO_2 within 6h of reaction at 150°C with equimolar FA to LA.[23] Among other screened oxides, the high interest of zirconia for supporting Au was recently confirmed in different operating conditions, *i.e.* small volume sealed glass tube instead of a pressurized reactor).[22] Ag and Ag-Ni catalytic systems were also studied,[24] and high efficiency with almost full LA conversion and full GVL yield was achieved over 10%Ag-20%Ni supported on zirconia at 220°C after 5 h of reaction.

Heterogeneous Ru-based catalysts were also proven to be efficient in the hydrogenation of LA with FA as a hydrogen source, and Heeres at al. interestingly showed that Ru/C catalyst was more active than its water soluble homogeneous Ru/TPPTS catalyst complex counterparts prepared *in situ* from $RuCl_3$ and sodium triphenylphosphine trisulfonate TPPTS.[25] They noticed that FA slowly decomposed in the reaction conditions, and suggested that the mechanism of this reaction should be investigated for obtaining deeper insight into the reaction network analysis.

Despite the above-described very promising results, the authors mostly concentrated on hydrogenation reaction and product yield, while there is no discussion about the reactions that might occur from the gas phase intermediates and their influence on the hydrogenation reaction. We believe however that they can be of significant importance, especially when using formic acid as a hydrogen source.

Formic acid decomposition has been shown to give two reaction pathways: dehydrogenation **(1)** to form H_2 and CO_2, and dehydration **(2)** to form H_2O and CO. In real reaction conditions however, the situation is much more complex. Subsequently, the water–gas-shift reaction (WGS) **(3)** can take place, as well as the Fischer-Tropsch reaction from the CO and CO_2 products in the presence of some catalysts like Ru **(4,5)**. CO_2 can also be reduced into CH_4 through the Sabatier reaction in which CO can be formed as by-product. Although less often mentioned, the formation of formaldehyde is possible due to the reaction of formate ions ($HCOO^-$) **(6)**.[26,27] However, those important issues of side reactions are mostly omitted by researchers and only very few such examples have been described.[28,29,30,31] While the side reactions decrease the hydrogen selectivity, CO is also a poison of the catalyst active centers. Therefore, the design of selective catalysts for this process still remains a challenge.

$$HCOOH \rightarrow H_2 + CO_2 \quad (1)$$
$$HCOOH \rightarrow H_2O + CO \quad (2)$$
$$CO + H_2O \rightarrow CO_2 + H_2 \quad (3)$$
$$CO + 3\,H_2 \rightarrow CH_4 + H_2O \quad (4)$$
$$CO_2 + 4\,H_2 \rightarrow CH_4 + 2\,H_2O \quad (5)$$
$$2\,HCOOH \rightarrow HCHO + CO_2 + H_2O \quad (6)$$

In our work, we concentrated on the synthesis of Ru catalysts by different preparation methods and discussed the influence of the properties of these catalysts on the LA hydrogenation with FA as internal hydrogen source. Particularly, we focused on the effect of chlorine on the catalyst surface and its influence on the activity. To draw a full picture, we combined catalytic tests, structural characterization and theoretical investigations. Considering the important role played by gas phase species resulting from FA decomposition and their influence on the hydrogenation reaction, the behavior of Ru catalysts in both FA dehydrogenation and LA hydrogenation with external hydrogen has been separately investigated in addition to the hydrogen transfer hydrogenation catalytic tests.

Experimental

Catalysts preparation

Ruthenium catalysts were prepared by incipient wet impregnation from hydrated $RuCl_3$ (Acros Organics) and $Ru(acac)_3$ (Sigma–Aldrich, 97%) methanolic solutions on high surface area C-DARCO® (Sigma-Aldrich) activated charcoal support. Catalysts prepared from $RuCl_3$ were reduced for 1 h in hydrogen at 200°C or 500°C, and labelled as Ru/C (Cl) LR and Ru/C (Cl) HR, respectively. Catalysts prepared from $Ru(acac)_3$ were first oxidized in air at 200°C for 2h and further reduced for 1 h in hydrogen at 200°C or 500°C, and labeled as Ru/C (AC) LR and Ru/C (AC) HR, respectively.

The Ru content in the Ru/C catalysts was obtained by inductively coupled plasma atomic emission spectroscopy (ICP-AES). The Ru wt.% of the Ru/C catalysts was 5 ± 0.3 %.

Characterization techniques

X-ray diffraction (XRD) measurements were carried out on a D8 Advance Bruker diffractometer, in a θ/θ mode and using the $K\alpha_1$ radiation of Cu at 1.5406Å.

X-Ray Photoelectron Spectroscopy (XPS) characterization was performed on a Multilab 2000 (Thermo) spectrometer equipped with Al $K\alpha$ anode ($h\lambda$=1486.6 eV). The energy shift due to electrostatic charging was subtracted using the graphitic carbon C 1s band at 284.6 eV. The spectra were decomposed assuming contributions with a Doniach–Sunjic shape[32] and a Shirley background subtraction.[33] Surface atomic ratios have been calculated using the sensitivity factors, as determined by Scofield.[34]

Transmission electron microscopy (TEM) was performed on a Topcon 002B microscope operating at 200 kV and with a point-to-point resolution of 0.18 nm. The sample was sonicated in ethanol before a drop of solution was deposited onto a holey carbon film on a Cu grid for observation.

ToF-SIMS measurements were performed using the ION-TOF GmbH instrument (TOF-SIMS IV) equipped with 25 kV pulsed Bi^+ primary ion gun in the static mode.

CO chemisorption measurements were performed in order to determine the average Ru particle size. They were done at room temperature with pulse technique with the PEAK-4 apparatus equipped with thermal conductivity detector[35] Before adsorption measurement, sample (0,2 g) was reduced for 1h in high purity H_2 flow at appropriate temperature. After reduction, the sample was cooled down to room temperature

Green Chemistry Accepted Manuscript

This journal is © The Royal Society of Chemistry 20xx

in Ar flow. Afterwards, CO pulses (0,05 ml) were introduced and the amount of adsorbed CO was derived from TCD analysis. Based on measured chemisorption, Ru particle size was calculated thanks to formula described in literature, [36] using a 0,6 CO:Ru stoichiometry.

Theoretical calculations

Density Functional Theory (DFT) calculations were performed using the Vienna Ab Initio Simulation Package VASP 5.3.5.[37,38] The exchange-correlation energies were calculated within the generalized gradient approximation, and with the Perdew Burke and Ernzerhof (PBE) functional.[39] Electrons-ions interactions were described by the Projector Augmented Wave method (PAW).[40,41] The Van-der-Waals interactions were modelised via the dDsC method.[42,43] An implicit model was used for the solvent.[44,45] The plane-wave extension was cut-off at 400 eV. The metallic surface was modelled by a four-layers p 4x4 slab, separated by five layers-equivalent of vacuum. The calculations have been performed at the Γ-point. Adsorptions and reaction processes were carried out on the upper layer of the slab. The top two layers of the surface and the adsorbates were relaxed during the simulations, until the forces were smaller than 0.015 eV/Å. However, the bottom two layers of the surfaces were kept fixed at bulk positions during the simulations, to mimic the bulk behaviour of a nanoparticle (interatomic distance of 2.70 Å). Adsorption energies were calculated as the difference between the energy of the adsorbed molecule on the surface with the energy of the bare surface and the one of the molecule in gas phase. The initial reaction pathway was obtained by linear interpolation with a mixed internal and cartesian coordinate system as implemented in Opt'n Path suite,[46] and then refined with the Nudge Elastic Band method.[47,48] Then, the corresponding transition state structure was obtained using the Dimer method.[49] We confirmed the TS by observing a single imaginary frequency which normal mode corresponds to the considered reaction coordinates.

Catalytic tests

Levulinic acid hydrogenation. In a typical levulinic acid (LA) hydrogenation experiment, 1 g of LA, 0.3 g of catalyst and 30 ml of water were combined in a stainless steel autoclave (Berghof, Germany), equipped with teflon insert allowing a reaction volume of 45 ml. The reactor was pressurized with H_2 to 10 bar and temperature was maintained at 190°C for 1 h. At the end of reaction, the reactor was cooled down, remaining pressure was released and reaction mixture was centrifuged to separate the solid catalyst and the product solution.

Formic acid decomposition. In a typical experiment, 2.0 ml of formic acid (FA), 0.3 g of reduced catalyst, and 30 ml of distilled water were combined in a stainless steel autoclave (Berghof) equipped with teflon insert allowing a reaction volume of 45 ml. The reactor was flushed with H_2 for 30 s and Ar for 15 s. The reactor was then heated to 190°C for 2 h.

LA hydrogenation with formic acid as a hydrogen source (FALA). In a typical LA hydrogenation experiment, 1 g of LA, 0.4-2 mL of FA, 0.3-0.6 g of a catalyst and 30 ml of water were combined in a stainless steel autoclave (Berghof), equipped with teflon insert allowing a reaction volume of 45 ml. The temperature was maintained at 190°C for 2-5 h. At the end of the reaction the reactor was cooled down, the remaining pressure was released and the reaction mixture was centrifuged to separate the solid catalyst and the product solution.

Reaction products analysis. In all cases, after the end of the reaction, the reactor was cooled down, the remaining pressure was released. Gaseous products were analyzed by gas chromatography (VEB Chromatrom, Berlin) equipped with the TCD detector. Argon was used as the carrier gas with a flow rate of 15 ml·min^{-1} and the injections were performed with a volume of 2 ml. Liquid products were analyzed by high-performance liquid chromatography (Perlan) equipped with refractive index detector and Rezex ROA column, 0.0025 mol·dm^{-3} H_2SO_4 was used as an eluent.

The liquid after reaction was analyzed by ICP-MS order to see whether leaching of active phase was taking place. In all cases it was proved that catalysts showed good stability during reaction conditions.

Results

Characterization by XRD, TEM, chemisorption and XPS.

Fig. 1 shows the powder XRD patterns of four Ru/C catalysts obtained from two different precursors, $RuCl_3$ Ru/C (Cl) and $Ru(acac)_3$ Ru/C (AC), and reduced at two different temperatures, a low one (200°C, LR) and a higher one (500°C, HR). The usual pattern of high surface area C DARCO® carbon support was observed, with the presence of broad diffraction peaks assigned to (002) and (101) planes of badly organized carbon, respectively.

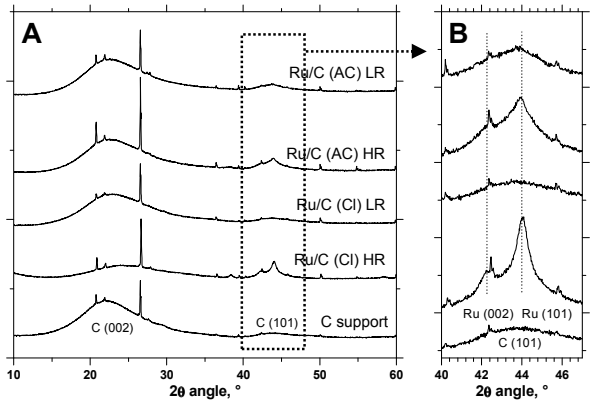

Fig. 1 Powder XRD pattern of Ru/C catalysts after reduction step at 200°C or 500°C, and of the bare high surface area carbon support. **(A)** Full diagram, **(B)** zoom on Ru (101) and Ru (002) diffraction peak zone, with overlap with the broad (101) peak of carbon.

In addition, non-resolved diffraction peaks attributed to bulk metallic Ru phase were observed at 42.2° and 44.0°, assigned

Green Chemistry Accepted Manuscript

to Ru (101) and Ru (002) diffraction planes (PDF-2, Card 00-006-0663, ICCD, 2004), respectively, except in the case of the Ru/C (Cl) reduced at the low temperature of 200°C. No diffraction peak was recorded on the Ru/C (Cl) LR sample probably due to a too small mean size of ruthenium particles and/or to their lower crystallinity. Estimating the average size of metallic Ru nanoparticles through usual Scherrer approximation would be too hazardous because of the overlap of both Ru diffraction peaks with broad (101) peak of carbon.

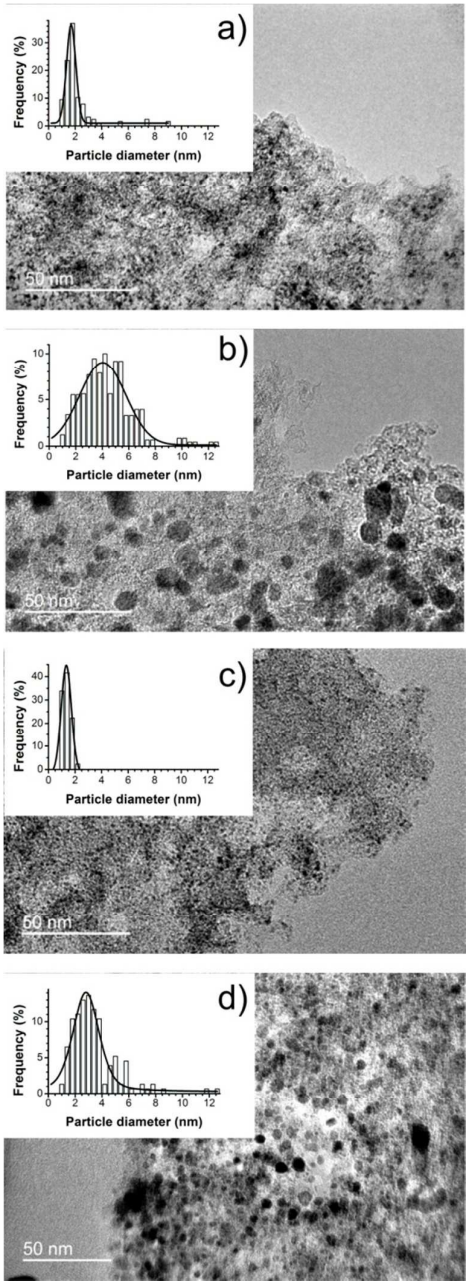

Fig. 2. TEM images and the corresponding metallic Ru nanoparticle size distribution histograms for Ru/C catalysts : **(a)** Ru/C (AC) LR, **(b)** Ru/C (AC) HR, **(c)** Ru/C (Cl) LR and **(d)** Ru/C (Cl) HR.

TEM measurements were used for analyzing size distribution of metallic Ru nanoparticles dispersed on the carbon support. Fig. 2 shows representative TEM images recorded on Ru/C catalysts, along with the corresponding Ru particle size distributions derived for more than 300 particles. The Ru/C (Cl) LR catalyst displayed a high metal dispersion with a mono-modal narrow particle size distribution and an average particle size of 1.3 nm. It was remarkable that no Ru nanoparticles larger than 2.2 nm were observed on this sample. A very good metal dispersion was obtained on the Ru/C (AC) LR catalyst, with a slightly broader particle size distribution, centered around 1.7 nm. By contrast, both catalysts reduced at the high temperature of 500°C displayed a lower and strongly less homogeneous metal dispersion on the carbon support. The Ru/C (Cl) HR catalyst displayed a broader average particle size of 2.8 nm, while it increased till 3.9 nm and broadened further on the Ru/C (AC) HR catalyst. It should be noted that – except for the Ru/C (Cl) LR catalyst with the best metal dispersion – bigger size ruthenium nanoparticles were observed by TEM beside the major contribution around which the particle size distribution is centred.

Similar behaviour was observed by CO chemisorption. The highest particle size was noted for Ru/C (AC) HR (5.4 nm) followed by Ru/C (AC) LR ≈ Ru/C (Cl) HR and the lowest for Ru/C (Cl) LR (0.9 nm) (Table 1). In the case of the catalysts prepared from the Cl precursor, the TEM and chemisorption sizes are rather similar.

In the case of catalysts prepared from acac precursor, the particle sizes derived from CO chemisorptions are in contrast significantly larger than those obtained from TEM. This difference could result from the partial decomposition of the acac precursor at 200°C,[50,51] leading to the presence of residual carbon deposit at the surface of the ruthenium crystallites and partially covering them.

Table 1 Ru nanoparticle size derived from CO Chemisorption and TEM measurements

Catalysts	Particle size from CO chemisorption [nm]	Particle size from TEM [nm]
Ru/C (AC) LR	2.9	1.7
Ru/C (AC) HR	5.4	3.9
Ru/C (Cl) LR	0.9	1.3
Ru/C (Cl) HR	2.8	2.8

XPS surface characterization has been performed for analyzing the ruthenium oxidation state, calculating the Ru/C surface atomic ratio and evidencing the presence of residual chlorine species in Ru/C (Cl) samples. Fig. 3 shows the ruthenium Ru *3p* region and the chlorine Cl *2p* region of XPS spectra recorded on the Ru/C catalysts. The binding energy overlap between both C *1s* and Ru *3d* region requires investigating preferentially the Ru *3p* secondary peak region.[52,53,54] However, the carbon C *1s* and ruthenium Ru *3d* region of XPS spectra is shown in supporting information SI 1.

Green Chemistry Accepted Manuscript

This journal is © The Royal Society of Chemistry 20xx

The Ru *3p* XPS spectra of Ru/C catalysts shown in Fig. 3A evidenced the presence of both metallic Ru^0 and Ru^{4+} in RuO_2 species at the surface, with the presence of two Ru $3p_{3/2}$ - Ru $3p_{1/2}$ orbital doublet contributions with spin orbit splitting of about 22 eV. It was worth noting that a shift of 0.7 eV towards higher energy was observed for Ru in both oxidation states in the case of the Ru/C (Cl) catalyst reduced at the low temperature of 200°C. Despite a more complex multi-contribution pattern, the C *1s* and Ru *3d* spectra confirmed the presence of both Ru-based phases, *i.e.* metallic Ru^0 (280.3 eV) and Ru^{4+} in RuO_2 (282.0 eV), with the appearance of two new Ru $3d_{5/2}$ - Ru $3d_{3/2}$ orbital doublet contributions with spin orbit splitting of about 4.1 eV, in addition to the contributions resulting from the carbon support material (Fig. S.I. 1).[55,56] Like for Ru *3p* spectra, the spectra of the Ru/C (Cl) LR sample evidenced a shift towards higher binding energies (here *ca.* 1 eV) for both doublet contributions corresponding to metallic Ru^0 and Ru^{4+}, *i.e.* at 281.3 eV and 283.0 eV, respectively.

This upward shift of both Ru *3d* and Ru *3p* orbital binding energies in the case of the Ru/C (Cl) catalyst reduced at the low temperature of 200°C, could be explained by an electron deficiency induced by the chemical environment of the ruthenium atoms, corresponding to the increase in effective positive charge around Ru^0 and Ru^{4+} surface species. This suggested the direct or indirect coordination of Ru atoms to strongly electron-withdrawing centers.

The chlorine Cl *2p* XPS spectra recorded on the catalysts prepared through the chloride way revealed the presence of residual chlorine species at the surface of the catalyst reduced at the low temperature of 200°C, *i.e.* Ru/C (Cl) LR (Fig. 3B). The presence of two different surface chlorine species could be suggested, taking into account a spin–orbit splitting of 1.6 eV for Cl $2p_{3/2}$ – Cl $2p_{1/2}$ doublet. Indeed, Mazzieri et al. reported that Ru oxychloride species characterized by $3d_{3/2}$ peak at 280.9 eV are present on the sample surface when using $RuCl_3$ as precursor for catalyst preparation.[57] One could thus hypothize that chlorine species remained after reduction at 200°C as ruthenium oxychloride phases. Whatever their nature, it can be possible that residual chlorine species remaining after reduction at 200°C at the surface of the catalyst could act as strongly electron-withdrawing centers for ruthenium atoms. Whether the interaction with ruthenium atoms is direct or indirect (through oxygen atom), the presence of chlorine at the surface of ruthenium nanoparticles could be responsible for the upward shift in binding energies observed for both Ru *3d* and Ru *3p* orbitals. Oxychloride species – or more generally chloride species evidenced by XPS – could result from partial decomposition/reduction of $RuCl_3$ precursor at the low temperature of 200°C, or from further room temperature oxidation of non-decomposed $RuCl_3$ during exposition to air.[58,59] By contrast, within the accuracy of the measurement, no residual surface chlorine was observed when the catalyst was reduced at the high temperature of 500°C, in agreement with the absence of any upward shift in binding energies for both Ru *3d* and Ru *3p* orbitals.

It was worth noting that the Ru/C catalysts loaded with 5 wt.% of Ru displayed different Ru/C surface atomic ratio, calculated via the Ru *3p* orbital XPS spectra. Both Ru/C (Cl) catalysts displayed strongly higher Ru/C surface atomic ratios than Ru/C (AC) catalysts, *i.e.* 0.62 and 0.53 for Ru/C (Cl) LR and Ru/C (Cl) HR, respectively, *vs.* 0.14 and 0.15 for Ru/C (AC) LR and Ru/C (AC) HR, respectively. Globally, the higher the Ru/C atomic surface ratio, the higher the dispersion of the Ru nanoparticles at the carbon support surface. However, the low values obtained for both catalysts prepared from acac – while the Ru/C (AC) LR sample has a small Ru particle size – resulted also probably from the presence of residual carbon deposit due to non-complete decomposition of acac precursor, in agreement with CO chemisorption/TEM analysis mentioned above. By contrast, in the case of Ru/C (Cl) LR, the presence of large amounts of chlorine species (as confirmed by ToF-SIMS analysis in Table 2) is probably responsible for the rather small difference in surface atomic ratios for both samples prepared with chloride precursor, despite a strongly different mean particle size derived from TEM.

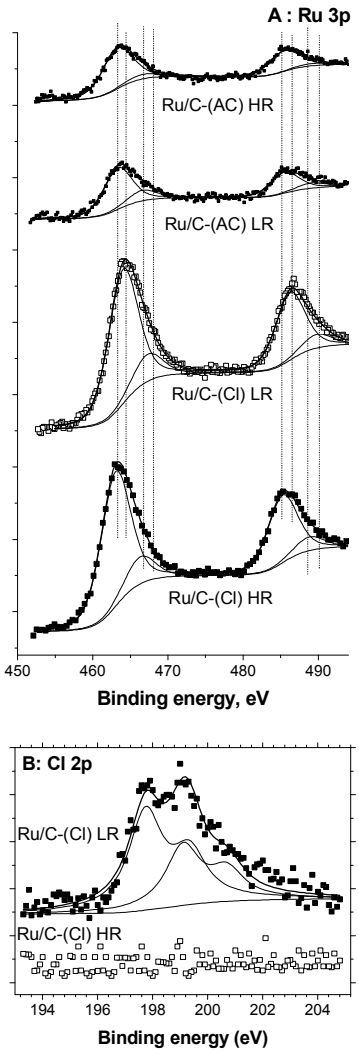

Fig. 3 (A) Ru *3p* and **(B)** Cl *2p* XPS spectra of the Ru/C catalysts.

Green Chemistry Accepted Manuscript

Time-of-Flight Secondary Ion Mass Spectrometry (ToF-SIMS) analysis. ToF-SIMS analysis of the catalysts surface was performed in order to identify what kind of the species is present on the surface of investigated materials. In Table 2, we demonstrate an intensity of ions normalized to the signal of oxygen. On the samples prepared from chlorine precursor, we identified ruthenium oxide, chlorine ions and ruthenium oxychloride species. The highest amount of chlorine was found in the case of Ru/C (Cl) LR, whereas significantly lower amount was identified for Ru/C (Cl) HR, which means that high temperature hydrogen treatment allowed for almost full removal of chlorine in accordance with the literature.[60] At the same time however it is possible to observe that high temperature treatment led to higher amount of accessible Ru in contrast to acac-derived catalysts for which no change was observed. In the case of acac samples, chlorine ions were identified as well – although in a much smaller quantity – and interestingly the same behavior was noticed and after high temperature reduction the amount of chlorine decreased significantly.

Table 2 Normalized intensity of ions calculated on the basis of ToF-SIMS spectra collected from the surface of Ru/C catalysts.

Ions	Ion intensity for Ru/C catalysts			
	Ru/C (Cl) LR	Ru/C (Cl) HR	Ru/C (AC) LR	Ru/C (AC) HR
Cl^-/O^-	2,9548	0,8424	0,2958	0,1451
RuO_2^-/O^-	0,0115	0,0213	0,0154	0,0147
RuO_3^-/O^-	0,0181	0,0317	0,0193	0,0200
RuO_2Cl^-/O^-	0,0212	0,0064	0,0024	0,0014

Temperature Programmed Reduction measurements. TPR profiles show several regions of H_2 consumption for the catalysts before the reduction (Fig. 4). For the catalyst prepared from chlorine precursor two peaks of maximum at 94°C and 155°C are probably related to the two reduction steps of the ruthenium chloride precursor, *i.e.* $Ru^{3+} \rightarrow Ru^{2+} \rightarrow Ru^0$.[61,62] We cannot exclude that the reduction of formed RuO_xCl_y species can occur in this region. In the case of catalysts prepared from acac precursor, the main reduction peaks are shifted into higher temperatures. There is one small broad effect with maximum at 114°C probably related to decomposition of acac precursor and three main peaks at temperatures of 217°C, 304°C and 509°C respectively. The effects at the highest temperatures for both catalysts are probably related to reduction of some carbon groups on the support, very probably around the metal particles. The peaks in the intermediate temperature region probably correspond to reduction of two different nanoparticles of RuO_2 amorphous or crystalline or just of two different nanoparticle sizes.

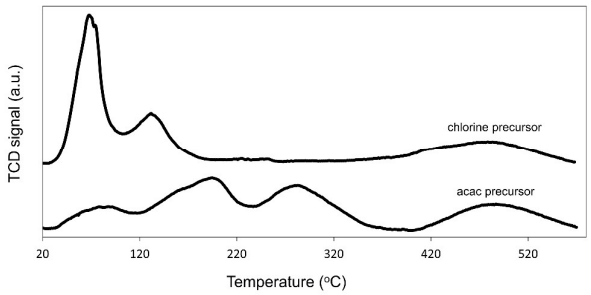

Fig. 4 Temperature programmed reduction profiles of 5%Ru/C catalysts prepared from different precursors.

Catalytic activity.

FA decomposition and LA hydrogenation on different metals. At first, FA decomposition and LA hydrogenation were performed independently with the same metal catalysts: Pd/C, Pt/C and Ru/C, all derived from an acetylacetonate precursor (Table 3). The highest catalytic performance in FA decomposition was observed over Ru/C (48% conversion). However in that case the formation of CH_4 was detected as well and therefore the selectivity to hydrogen was lower. Even though methane formation was not observed in the case of Pd and Pt, those catalysts were less active. On the other hand, Ru/C catalyst also showed the highest activity in LA hydrogenation, followed by Pd and Pt. This phenomenon was already explained in our earlier work that for oxophilic metals like Ru in aqueous environment the effective energy barrier is decreased making them more active.[13]

Table 3 Activity of selected metal catalysts in individual reactions: LA hydrogenation with external hydrogen and FA decomposition.

Catalyst[1]	LA hydrogenation[2]		FA decomposition[3]				
	GVL yield [%]	LA conversion [%]	FA conversion [%]	Gaseous product amount [% vol]			
				H_2	CO	CH_4	CO_2
Pd/C	35	46	23	53	13	0	34
Pt/C	18	30	31	57	11	0	32
Ru/C	75	87	48	26	9	9	56

[1] All catalysts were prepared by using $Me(acac)_x$ as a metal precursor, where Me is Pd, Pt and Ru (reduction temperature of 200°C)

[2] Reaction conditions: 190°C; 2 h; 0,3 g of catalyst; 1 g of LA; external source of hydrogen (10 bar), water as a solvent

[3] Reaction conditions: 190°C; 0,3 g of catalyst ; 2 h; 2 ml of FA, water as a solvent, autogenic pressure

When it comes to the distribution of gaseous products, it is possible to observe that FA is decomposed most probably *via* two pathways, *i.e.* dehydration and dehydrogenation, leading to the formation of both CO and CO_2, even if we can not ruled out the possible formation of CO by reverse water-gas-shift (RWGS) reaction. There is also a high probability of methane formation as a secondary reaction, especially in the case of Ru.

Green Chemistry Accepted Manuscript

This journal is © The Royal Society of Chemistry 20xx

In the simultaneous FA decomposition and LA hydrogenation towards GVL performed in the same conditions, the order of activity among tested materials was the same, no GVL yield being however obtained (Table 4). The LA conversion was observed only due to its adsorption on the carbon surface, which was confirmed by additional tests, provided as Supporting Information SI 2. Also no change in the distribution of gaseous products was noted. The highest hydrogen yield was present thanks to higher FA conversion.

Table 4 Activity of metal catalysts in simultaneous FA decomposition and hydrogen transfer reaction to LA hydrogenation.

Catalyst	GVL yield [%]	LA conversion [%]	FA conversion [%]	Gaseous product amount [% vol]			
				H_2	CO	CH_4	CO_2
Pd/C	0	10	15	43	12	2	43
Pt/C	0	0	19	nd	nd	nd	nd
Ru/C	0	7	48	24	16	2	58

Reaction conditions: 190°C; 0,3 g of catalyst ; 2 h; 1 g of LA; 2 ml of FA, 30 ml of water as a solvent, autogenic pressure. nd – not determined.

For the following, we decided to focus on Ru-based catalysts since it shows the highest activity in both reactions. In order to increase the conversion and to achieve GVL formation in the LA hydrogenation with FA as internal hydrogen source, two strategies were implemented: first the optimization of the amount of solvent, and the second the influence of the Ru/C catalyst preparation method.

Influence of the amount of solvent. Table 5 shows that higher conversion values were reached when less solvent was used. While FA decomposition in gas phase is close to zero order, it is not the case anymore for liquid phase, which can explain the difference in the results. The resulting gas phase composition results from a subtle balance between several competitive reactions.

Table 5 Influence of the amount of solvent in simultaneous FA decomposition and hydrogen transfer reaction to LA hydrogenation on Ru/C catalyst.

Solvent amount [ml]	GVL yield [%]	LA conversion [%]	FA conversion [%]	Gaseous product amount [% vol]			
				H_2	CO	CH_4	CO_2
5	33	49	99	4	10	12	74
15	21	43	92	13	8	8	71
30	0	11	88	11	9	9	71
40 [1]	0	0	61	-	-	-	-

[1] due to low FA conversion and therefore low build-up pressure, analysis of gaseous products was not possible.

Reaction conditions: 190°C; 0,3 g of catalyst ; 2 h; 1 g of LA; 2 ml of FA, water as a solvent, autogenic pressure, Ru/C (AC) LR catalysts.

The case with only 5ml of water added is an extreme case where a minimal amount of liquid phase was used. Then, the diffusion to active sites of the catalysts can be facilitated and the decomposition of FA proceeds much faster. Therefore, a much higher LA conversion was observed in those conditions, which was accompanied by GVL formation 33 % GVL yield. On the other hand, high amounts of methane and CO were also formed. Due to a low amount of water probably the WGS reaction was less facilitated, which could be the origin of higher CO amount.

The case with 40mL corresponds to the other extreme with a reactor almost full of liquid where no pressure can build-up.

Influence of the Ru/C catalyst preparation method. Our second approach to boost the reaction performance was related to understanding the behavior of different Ru catalysts, derived from two precursors, $RuCl_3$ and $Ru(acac)_3$ named Ru/C (Cl) and Ru/C (AC) respectively. They were reduced at two different temperatures, 200°C (LR) and 500°C (HR).

The four different Ru catalysts were tested separately in FA decomposition and LA hydrogenation (Table 6). In FA decomposition, the highest activity was noticed for Ru/C (Cl) HR where full conversion was reached after 1 h of the reaction, whereas by contrast activity was much lower for the catalyst reduced at a lower temperature. The same trend was observed for catalysts prepared from acac. The higher reduction temperature treatment gave very active catalysts (79% of FA conversion) whereas low temperature treatment formed catalysts with lower activity.

The situation was different in LA hydrogenation performed with external hydrogen source where there was almost no activity difference for all tested materials.

Table 6 Activity of Ru/C catalysts in individual reactions: LA hydrogenation with external hydrogen and FA decomposition.

Catalyst	**LA hydrogenation**		**FA decomposition**					
	GVL yield [%]	LA conversion [%]	FA conversion [%]	P (bar)	Gaseous product amount [% vol]			
					H_2	CO	CH_4	CO_2
Ru/C (AC) LR	74	88	38	30	13	11	3	73
Ru/C (AC) HR	68	81	79	50	18	17	10	55
Ru/C (Cl) LR	72	86	69	45	8	10	17	65
Ru/C (Cl) HR	75	87	100	70	10	7	18	65

Reaction conditions:FA decomposition: 190°C; 0,3 g of catalyst; 2 ml of FA; 1h; autogenic pressure. LA hydrogenation : 10bar H_2 1 g of LA, 0,3 g of catalyst water as a solvent

In the following step, Ru catalysts were tested in simultaneous FA decomposition and LA hydrogenation. In Table 7, the results of this reaction after 2 and 5 h are presented. The order of activity in this reaction follows the FA decomposition (Table 6). The highest GVL yield was reached over both catalysts derived from a chlorine precursor (the same rate of GVL yield increase was observed for both Ru/C (Cl) catalysts).

Green Chemistry Accepted Manuscript

The highest increase of GVL yield after 5 h of reaction in respect compared to its value after 2 h was observed for samples that had little or no conversion after 2 h, namely the two acac-derived catalysts Ru/C (AC). For the catalysts derived from the acetylacetonate precursor, full conversion of FA was necessary before the reduction of LA could proceed (Table 7).

Table 7 Activity of Ru/C catalysts in simultaneous FA decomposition and hydrogen transfer reaction to LA hydrogenation

Catalyst	Reaction time [h]	GVL yield [%]	LA conversion [%]	FA conversion [%]	Gaseous product amount [% vol]			
					H_2	CO	CH_4	CO_2
Ru/C (AC) LR	2	0	11	88	11	9	9	71
	5	31	50	100	4	9	14	72
Ru/C (AC) HR	2	13	36	100	13	7	14	66
	5	45	67	100	6	4	22	68
Ru/C (Cl) LR	2	24	52	85	11	12	13	64
	5	46	62	100	5	13	12	70
Ru/C (Cl) HR	2	41	66	100	17	9	15	60
	5	57	81	100	7	15	16	62

Reaction conditions: 190°C; 0,6g of the catalyst; 1g of LA; 2 ml of FA, 30 ml of water as a solvent, autogenic pressure.

As the catalysts obtained from Cl-containing precursor were very active and FA conversion was proceeding fast, more detailed studies were carried out for better understanding the formation of products during reaction time. Therefore on Fig. 5 a more complete reaction performance is shown.

In the case of Ru/C (Cl) HR (Fig. 5a), in the first step FA is decomposed and already after 15 min 80% of conversion is achieved. During this period, the highest variations in the gaseous products distribution are observed. The methane formation increases, and similarly the yield of CO_2 and CO are the highest, which suggests that methane is formed *via* two possible pathways: $CO + 3\ H_2 \rightarrow CH_4 + H_2O$ and $CO_2 + 4\ H_2 \rightarrow CH_4 + 2H_2O$. Interestingly, once FA is fully decomposed, the methane formation seems to be limited, a change of regime is observed and the formation of GVL starts. The difference between LA conversion and GVL formation yield is due to adsorption of LA on the catalysts surface (see supporting information SI 2).

In the case of Ru/C (Cl) LR, the main difference is related to the fact that FA decomposition occurs very slowly and conversion of 80% is reached only after 60 min of the reaction. Another difference is that GVL yield is observed already with very low conversions of FA (*e.g.* after 10 min of reaction, FA conversion is 27% and 2% GVL was noted). The GVL yield is very low and until 80% FA conversion never reached more than 5%. Then, a significant increase is observed (Fig. 5).

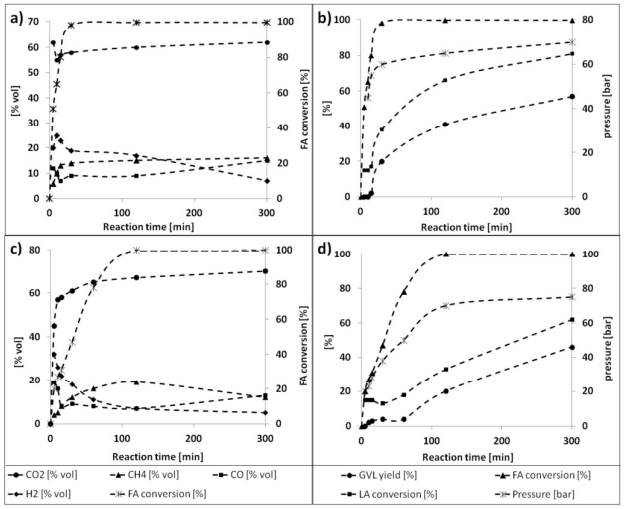

Fig. 5 Product distribution as a function of reaction time for **(a,b)** Ru/C (Cl) HR and **(c,d)** Ru/C (Cl) LR.

Similar behavior for these catalysts was however noticed in the case of gaseous products formation, the maximum uptake of CO and H_2 together with the formation of CH_4 were observed until the full conversion of FA was reached.

A question arises why the hydrogenation of LA proceeds in some cases only to a small extent or does not start at all before the FA is fully decomposed. In order to understand this, the following test was performed: hydrogenation of LA was carried out in the same conditions under the same hydrogen pressure but additionally FA was added (Table 8). In this case the LA conversion was much lower (25%) than in the hydrogenation without FA where almost double conversion was reached. Similar effect was observed where instead of FA CO_2 was introduced together with H_2 and surprisingly the results were similar like in the case of the addition of FA.

Table 8 Activity of the 5%Ru/C (Cl) HR catalyst in simultaneous FA decomposition and hydrogen transfer reaction to LA hydrogenation.

Reaction time [min]	H_2 pressure (bar)	CO_2 pressure (bar)	GVL yield [%]	LA conversion [%]	FA conversion [%]	Gaseous product amount [% vol]			
						H_2	CO	CH_4	CO_2
300	25	25	56	84	-	11	12	14	63
300	-	-	57	81	100[(1)]	7	15	16	62
30	25	-	82	99	-	-	-	-	-
10	5	-	4	25	62[(2)]	-	-	-	-
10	5	-	32	45	-	-	-	-	-

Reaction conditions: 190°C; 0,3 g of catalyst; 1g of LA; 30 ml water as a solvent; [(1,2)] 2 ml of FA.

Green Chemistry Accepted Manuscript

This journal is © The Royal Society of Chemistry 20xx

Theoretical Calculations.

Theoretical calculations of possible reaction paths were performed in order to better understand the experimental observations on the levulinic acid hydrogenation using the formic acid as a hydrogen source.

In particular, we aimed at understanding the chlorine effect on this global reaction and on the separate reactions, namely the formic acid decomposition into H_2 and CO_2 and the hydrogenation of LA. This latter is followed by an intra-molecular esterification to yield GVL that is not catalyzed by the metallic supported catalyst. We therefore used two models: Ru and chlorinated Ru (Cl-Ru). Since the larger nanoparticles after high temperature reduction are more active in our case, the active sites are probably not located on edges and corners but on the most stable facet, the Ru(0001). In addition, the decomposition of the formic acid has been shown to be more efficient on Ni(111) than on Ni(211) by DFT calculations.[63] So we modeled the catalysts by (0001) slabs. Cl-Ru includes a coverage of 1/4 ML of Cl: on a p(4x4) cell, four atoms of chlorine are adsorbed on a fcc position, maximizing the distance between them. The water solvent is taken into account by a continuum model. The coordinates of the structures are all provided in Supporting Information SI 3.

Comparative adsorption. During the hydrogen transfer process, two reactions are competing: the dehydrogenation of formic acid and the hydrogenation of the levulinic acid. They can occur simultaneously or sequentially depending on the relative adsorption of the reactants. Formic acid adsorbs strongly and dissociatively on Ru (-1.76 eV) and Cl-Ru (-1.58 eV) and occupies two Ru sites under this formate form. Acetone (as a levulinic acid model) adsorbs less strongly (Ru, -1.30 eV ; Cl-Ru -0.87 eV) despite the inclusion of a stabilizing water molecule. Its hydrogenation requires also the dissociative adsorption of H_2. Considering the reaction: $H_2 \rightarrow 2H_{ads}$, the H_2 adsorption is of -1.22 eV on Ru and of -0.86 eV on Cl-Ru. Here again, the chlorination destabilizes the adsorbed hydrogen atom that sits preferentially at a fcc site. The decrease in adsorption energy can be related to the lowering of the d band center of the Ru in presence of Cl (see Supporting Information SI 3 for a plot of the density of state projected on the d orbitals of the Ru top layer). The comparison of those adsorption energies is in favor of a surface covered by formate at low conversion in formic acid, and this is limiting the subsequent ketone hydrogenation. This explains the previously presented results of hydrogenation of LA with H_2 in the presence of FA or in presence of CO_2 (vide supra, Table 8). The formic acid adsorbs dissociatively under its formate form and blocks the adsorption of the LA or H_2. It inhibits the hydrogenation reaction. Similarly, under a pressure of H_2, the added CO_2 can lead also to surface formate, which here again blocks the LA hydrogenation reaction.

Formic acid decomposition. Two paths are possible for the formic acid dehydrogenation into CO_2. In the formate path, the OH bond breaks, first yielding HCOO as an intermediate while the carboxyl path starts with the CH cleavage that produces the COOH intermediate. The two reaction paths are similar on the Ru(0001) and the Cl-Ru(0001) surface and in line with previous DFT results on Ru[64] and other metals.[65,66] The corresponding energy profiles are shown in Fig. 6.

Most of the structures are not affected by the chlorination of the Ru surface. In its most stable configuration, the formic acid adsorbs in a top position with the carbonyl O directly on top of a surface atom (Ru-O = 2.15 Å), and the H of the hydroxyl group is facing downward toward the surface. This is not affected by the chlorination of the Ru(0001) surface. This configuration is a natural starting point for the formate pathway that starts with the O-H breaking. The corresponding transition state (TS) is a classical three-center transition state

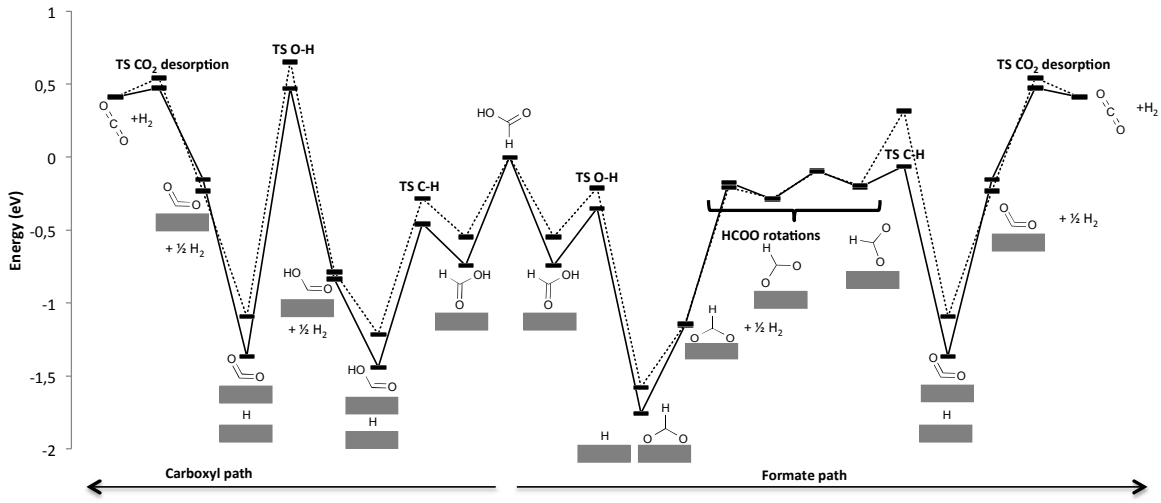

Fig. 6 Energy profile (in eV) for FA dehydrogenation on Ru (full line) and Cl-Ru (dashed line)- the reference is HCOOH in gas phase and bare slabs.

Green Chemistry Accepted Manuscript

with a OH bond distance elongated by 46% at 1.44 Å on Ru(0001) and by 44% at 1.44 Å on Cl-Ru(0001). On both catalysts, the resulting formate HCOO adsorbs in a bidentate manner, bridging two adjacent Ru surface atoms (Ru-O= 2.10 Å). The next step is the C-H breaking to yield CO_2 and a second hydrogen atom adsorbed on the surface. This first step requires to break one Ru-O bond and then to rotate the HCOO till the CH bond points toward the surface, as underlined already by the group of Luo et al. on the metals of group VIII[66] and ourself on Ni in electrochemical conditions.[67] This rotation is followed by the CH bond dissociation via a late type transition state. The resulting CO_2 is chemisorbed in a di-σ manner and strongly bended and its desorption is an activated process as already previously shown.[67] The other possibility for dehydrogenating HCOOH is to break the C-H bond first, then the O-H (carboxyl path on the left of Fig. 6). The C-H breaking goes through a three-center transition state with a C-H bond that is not much elongated yet (1.13 Å, 1.14 Å on Ru-Cl) but a Ru-C bond that is already rather short (2.51 Å). The resultant carboxyl intermediate COOH adsorbs in a di-σ manner, the C=O parallel to a Ru-Ru bond and the C-OH almost perpendicular to the surface plane. Then, the O-H cleavage goes through 3-centers TS, with an O-H bond 1.46 Å, 1.42 Å on Ru-Cl long, yielding the chemisorbed CO_2 and a hydrogen atom.

Just like the structures, the energy landscape of HCOOH dehydrogenation is not much disturbed by the addition of Cl atoms on the surface. The chlorination slightly destabilizes most of the surface species. The most impacted is the formic acid adsorption, weakened by 0.20 eV (from -0.74 eV to -0.54 eV). This is in line with the hydrogen destabilization of 0.18 eV. On both paths, the mono-dehydrogenated intermediate is the most stable species along the path and its energy is not strongly impacted by the addition of chlorine atoms, even at a coverage of 1/4ML. In addition, the formate is around 0.3 eV more stable than the carboxyl intermediate. Breaking the CH bond in the formate is easier than breaking the OH in the carboxyl intermediate on Ru (activation energy of 1.08eV vs 1.31eV) As a result, the preferred path is clearly the formate path on Ru(0001). This is in line with the results already published on Ni(111) by Luo et al.[66] and by Herron et al.[68] However, on Cl-Ru, the situation is different. The chlorination destabilizes more strongly the CH bond dissociation transition state than the other species. This leads to a strong increase of the resulting activation barrier (1.46 eV). The formyl path is less affected with a barrier around 1.44 eV. Finally, compared with bare Ru, the FA dehydrogenation is made more difficult on the chlorinated surface with an increase of the rate-determining barrier of 0.36 eV.

Hydrogenation of the ketone function. The second step of the catalytic hydrogen transfer is the hydrogenation of the ketone function of LA. Since only the ketone part of the LA is transformed during the hydrogenation step, we have modeled this bi-functional molecule by a simpler model, the acetone. To properly describe the hydrogenation ability of Ru, we have recently shown that it is necessary to include at least one water molecule chemisorbed on the metallic surface.[13] We kept this solvent model here and included also the bulk effects through the inclusion of a continuum model. To further improve our model, we added also a dispersion correction. The difference in the energetic one may notice between this work and our previous study[13] can be imputed to the larger cell used here, the different K point mesh chosen and the improvements to evaluate the energy. Here again, two reaction paths are possible. In the alkoxy path, the hydrogenation starts with the carbon yielding an alkoxy intermediate while in the hydroxy-alkyl path, it starts with the hydrogenation of the oxygen. The energy profiles on both Ru and Cl-Ru are shown in Fig. 7.

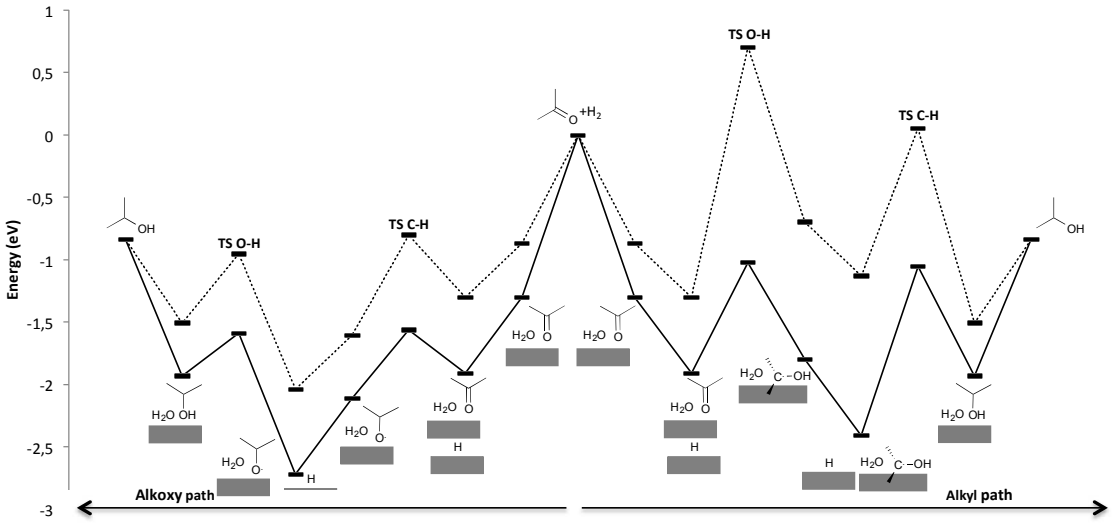

Fig. 7 Energy profile (in eV) for Acetone dehydrogenation on Ru (full line) and Cl-Ru (dashed line) - the reference is the acetone in gas phase, a H_2 molecule in gas phase, a bare slab and a hydrated slab with an H_2O molecule adsorbed on it.

Green Chemistry Accepted Manuscript

This journal is © The Royal Society of Chemistry 20xx

The structures are similar to the ones we obtained with a slightly different set up on Ru[13] and are not strongly affected by the presence of the chlorine atoms. In its most stable configuration, acetone adsorbs in a top manner, via the oxygen atom, and forms an H bond with the water molecule adsorbed on a neighbour Ru atom (Ru-O 2.17 Å, H-bond 1.67 Å). The final iPrOH is physisorbed accepting a 1.57 Å H-bond from the water. The hydroxyl-alkyl path starts with the O hydrogenation. In the corresponding three-centers TS, both the C and the O atom are interacting with Ru surface atoms, and the water is on a neighbour atom, assisting through a H-bond. Its structure is not strongly affected by the chlorination: the O-H distance is only slightly elongated on Ru-Cl (1.39 Å *vs.* 1.37 Å). Then, the surface hydroxyl-alkyl radical adsorbs in a disigma manner on both the Ru and the Cl-Ru and undergoes the second hydrogenation on the C center. In the corresponding transition state, the forming C-H is clearly more elongated on Ru-Cl than on Ru (1.97 Å *vs.* 1.67 Å). The alkoxy path starts with the C hydrogenation. Here again, the forming C-H is noticeably longer on Ru-Cl than on Ru (1.87 Å *vs.* 1.61 Å). The surface isopropoxy iPrO is adsorbed on a bridge site on Ru. In presence of ¼ ML of chlorine, it is pushed in a top position to reduce the repulsive interactions with the chlorine in fcc sites. For the next hydrogenation, the TS look alike on both surfaces with the O atom on a top site and a 1.39 Å H-bond with the water sitting on a neighbour site, on both catalysts.

In opposite to the HCOOH, the acetone hydrogenation energy landscape is at first sight strongly disturbed by the Cl presence. The chlorination strongly destabilizes all the surface species by around 0.5 eV as easily seen on Fig. 7. For instance, the adsorption energy of the ketone is reduced by 0.43 eV (-1.30 eV *vs.* -0.87 eV on Ru and Cl-Ru respectively) and so does the one of the final alcohol (-1.10 eV *vs.* -0.67 eV on Ru and on Cl-Ru respectively). On the hydroxyl-alkyl path, the chlorination disturbs greatly the first O-H formation. However this is not the preferential path nor on Ru nor on Cl-Ru, *i.e.* this influence just makes the hydroxyl-alkyl path even less favorable, if impossible since 2 eV is a rather high activation energy for usual reaction conditions. Acetone hydrogenation takes place through the alkoxy path on both catalysts. On this path, the presence of ¼ ML of chlorine destabilizes both the intermediates and the transition states with the *same* magnitude, meaning the effective barrier will remain basically the same. Along this path, the rate-limiting step is the second step. In a strong contrast with the O hydrogenation of the hydroxyl-alkyl path, the chlorination of the surface here decreases only slightly the activation barrier from 1.13 eV on Ru to 1.08 eV on Cl-Ru. Since this step is the rate-limiting one, the chlorination is not expected to strongly affect the hydrogenation reaction.

Discussion

In the hydrogenation of levulinic acid into γ-valerolactone with formic acid as a hydrogen source, one difficulty is to find a catalyst able to perform equally well for both reactions: the formic acid dehydrogenation and the levulinic acid hydrogenation. We started this study comparing several metals for the separated reactions and the hydrogen transfer. The three selected metals (Pd,Pt,Ru) succeeded in the dehydrogenation of formic acid in absence of levulinic acid and in the hydrogenation of levulinic acid under a pressure of H_2. For both reactions, the Ru/C is the most efficient catalyst. Then, in the hydrogen transfer conditions, Ru/C is even the only one to keep a similar conversion in formic acid, but with no production of GVL. Those preliminary results triggered us to investigate how the catalytic conditions but also the preparation of the Ru/C could be optimized for this challenging hydrogen transfer process.

We have investigated the influence of different preparation methods of Ru/C catalysts. With all of them, it is striking that a high conversion of formic acid is required before the LA hydrogenation can take place. In addition, we have demonstrated that the addition of formic acid or of CO_2 to the catalytic test of the levulinic hydrogenation reduces considerably the catalytic efficiency (see Table 8). This can be rationalized by the relative adsorption of the reactants computed by DFT. Formic acid can easily and strongly adsorbs dissociatively on Ru(0001) under its formate form according to surface science study at temperature as low as -193°C.[69,70,71] This is in agreement with our DFT calculations. In addition, Meng et al. have also shown that there is a stabilizing interaction between two surface formate on Ru(0001) combining mean-field kinetic model with both the transient thermal desorption and isothermal desorption spectra.[72] Comparatively, the levulinic acid (here modeled by acetone) and the dihydrogen have a much weaker energy of adsorption (cf. DFT results presented here). Consequently, the catalyst surface is fully covered by formate until a high enough conversion is reached in formic acid dehydrogenation, liberating catalytic sites for H_2 and the ketone. In other words, formate acts as a inhibitor for the LA hydrogenation.

The choice of the temperature (low or high) of reduction and the precursor (Cl or acac) had a strong influence on the catalytic performance, but the rationalization of those parameters influences is far from trivial. The activity in hydrogen transfer cannot be directly related with simple parameters as the mean size of the particles or the presence/absence of chlorine on the surface.

To rationalize the different activities that we observed, we combined catalytic tests, structural characterization and theoretical investigations. In addition to the catalytic tests performed for the hydrogen transfer process, we considered also the formic acid dehydrogenation and the hydrogenation of the levulinic acid in two separate catalytic tests. Our goal is to separate the chlorination effect from the structural effect.

Let's start with the Ru catalysts derived from the $RuCl_3$ precusor. It is known that presence of chlorine can change the metal particle dispersion together with resistance to thermal sintering. It can increase the mobility of metal oxide, and in that case it can accelerate both sintering and redispersion.[73,74] Thus, we cannot simply de-correlate the chlorination effect from the dispersion. To separate the chlorination effect from

Green Chemistry Accepted Manuscript

the number of accessible sites, we studied the formic acid decomposition and the hydrogenation of LA by the mean of DFT on two different models: the bare Ru(0001) surface and a chlorinated Ru(0001) surface (1/4ML in Cl). The chlorination lowers the d band center of the Ru, modifying the nature of the active sites and leading to a lower adsorption of most surfaces species. This modification of the Ru is also observed experimentally by XPS since the binding energy of the Ru levels is higher for the highly chlorinated Ru/C (Cl) LR. Based on a detailed mechanistic study on those models, we concluded that the presence of chlorine inhibit the HCOOH dehydrogenation reaction, pushing up in energy the transition state of the rate-limiting CH cleavage from the formate intermediate. In contrast, the rate-limiting step of the hydrogenation of the ketone function (here modeled by acetone) is not strongly affected. This is in line with our experimental observations since the LA hydrogenation is not sensitive to the chlorination while the higher content in chlorine is related to lower catalytic efficiency in formic acid dehydrogenation when considering the two Ru/C (Cl) catalysts.

We consider now the case of the two catalysts derived from the same acac precursor but reduced at two different temperatures. Those catalysts cannot contain more than traces of chlorine. Hence, the difference in activity in formic acid dehydrogenation we observed cannot be related to the presence or absence or chlorine. Nevertheless, here again the catalyst reduced at a higher temperature is more much active in formic acid dehydrogenation. This might be related to the increase in the crystallite size (from 2.9 nm to 5.4 nm upon the increase in reduction temperature, as measured by CO chemisorption). This increases is related to a lower number of active sites but with a greater activity of the catalyst in formic acid dehydrogenation. This means that the H_2 production from HCOOH may be favored by the greater extent of (0001) facets as it has been demonstrated by DFT calculations on other oxophilic metallic surfaces (Ni(111) *vs.* Ni(211)).[63]

Last, the comparison of the catalysts obtained from the chlorinated precursor and the one derived from the acac precursor shows that the acac one is less active than the (Cl) one for a given temperature of reduction. A plausible explanation is that the acac precursor could be a source of poisoning species that partially cover the surface by carbon deposit. We are however limited by the selection of calcination temperature range due to presence of active carbon used as a support. This is in agreement with the strong reduction in surface ratio as semi-quantitatively observed by XPS and with the higher size of particles obtained by chemisorption than by TEM. TPR results also confirm the presence of small residue of acac for the catalysts after temperature treatment in air. So, the the number of active site for a given "size" is much lower than expected, explaining the reduced catalytic activity of the acac-derived catalysts compared with the chlorinated one.

Conclusions

To conclude, varying the temperature reduction and the precursor of Ru/C catalysts, we demonstrated that the kind of the preparation method of the catalyst can greatly influence its activity in the levulinic acid conversion into GVL using formic acid as a hydrogen source. Despite an extensive characterization complement by DFT modeling, the comparative activity is not completely understood yet. We showed a clear poisoning of the presence of chlorine when using $RuCl_3$ as a precursor combining catalytic tests, XPS and ToF-SIMS analysis and reaction paths modeling. It seems also that this process could be structure sensitive, favored on larger particles and that the carbon support is affected by the condition of preparation of the catalysts. Last, the analysis of the relative adsorption energies of formic acid, levulinic acid and H_2 shows that the poisoning of the surface by formate is at the origin of the delay in levulinic acid hydrogenation in presence of formic acid.

Acknowledgements

Authors acknowledge the support of the Polonium project "Hydrogen transfer reactions for biomass transformation". Vasiliki Papaefthimiou (ICPEES) is thanked for performing XPS analysis.

Notes and references

1 W. Luo, M. Sankar, A.M. Beale, Q. He, C.J. Kiely, P.C.A. Bruijnincx and B.M. Weckhuysen, *Nat. Commun.*, 2015, **6**, 6540-6549.
2 M. Besson, P. Gallezot, C. Pinel, Chem. Rev., 2014, 114, 1827.
3 I.T. Horvath, H. Mehdi, V. Fabos, L. Boda and L.T. Mika, *Green Chem.*, 2008, **10**, 238.
4 D.M. Alonso, S.G. Wettstein and J.A. Dumesic, *Green Chem.*, 2013, **15**, 584.
5 L.E. Manzer, *Appl. Catal. A: Gen.*, 2004, **272 (1-2)**, 249-256.
6 I. Obregón, E. Corro, U. Izquierdo, J. Requies and P.L. Arias, *Chin. J. Catal.*, 2014, **35(5)**, 656-662.
7 K. Yan, T. Lafleur, G. Wu, J. Liao, C. Ceng and X. Xie, *Appl. Catal. A: Gen.*, 2013, **468**, 52-58.
8 P.P. Upare, J.M. Lee, D.W. Hwang, S.B. Halligudi, Y.K. Hwang and J.S. Chang, *J. Ind. Eng. Chem.*, 2011, **17(2)**, 287-292.
9 W. Luo, U. Deka, A.M. Beale, E.R.H. van Eck, P.C.A. Bruijnincx and B.M. Weckhuysen, *J. Catal.*, 2013, **301**, 175-186.
10 M.G. Al-Shaal, W.R.H. Wright and R. Palkovits, *Green Chem.*, 2012, **14**, 1260-1263.
11 A.M.R. Galletti, C. Antonetti, V. De Luise and M. Martinelli, *Green Chem.*, 2012, **14**, 688-694.
12 A.M. Ruppert, J. Grams, M. Jędrzejczyk, J. Matras-Michalska, N. Keller, K. Ostojska and P. Sautet, *ChemSusChem*, 2015, **8(9)**, 1538-1547.

Green Chemistry Accepted Manuscript

This journal is © The Royal Society of Chemistry 20xx

13 C. Michel, J. Zaffran, A.M. Ruppert, J. Matras-Michalska, M. Jędrzejczyk, J. Grams, and P. Sautet, *Chem. Commun.*, 2014, **50**, 12450-12453.
14 C.Michel, P. Gallezot, *ACS Catalysis*, 2015, **5**, 4130-4132
15 D.J. Braden, C.A. Henao, J. Heltzel, C.T. Maravelias, and J.A. Dumesic, *Green Chem.*, 2011, **13**, 1755-1765.
16 L. Corbel-Demailly, B.K. Ly, D.P. Minh, B. Tapin, C. Especel, F. Epron, A. Cabiac, E. Guillon, M. Besson and C. Pinel, *ChemSusChem*, 2013, **6**, 2201-2213.
17 C. Ortiz-Cervantes and J.J. García, *Inorg. Chim. Acta*, 2013, **397**, 124-128.
18 H. Mehdi, V. Fábos, R. Tuba, A. Bodor, L.T. Mika and I.T. Horváth, *Top. Catal.*, 2008, **48**, 49-54.
19 L. Deng, J. Li, D.M. Lai, Y. Fu and Q.X. Guo, *Angew. Chem. Int. Ed.*, 2009, **48**, 6529-6532
20 X. Tang, X. Zeng, Z. Li, L. Hu, Y. Sun, S. Liu, T. Lei and L. Lin, *Renewable and Sust. Energ. Rev.*, 2014, **40**, 608-620.
21 X.L. Du, L. He, S. Zhao, Y.M. Liu, Y. Cao, H.Y. He and K.N. Fan, *Angew. Chem. Int. Ed.*, 2011, **50**, 7815 –7819.
22 P.A. Son, S. Nishimura and K. Ebitan, *RSC Adv.*, 2014, **4**, 10525
23 X.L. Du, L. He, S. Zhao, Y.M. Liu, Y. Cao, H.Y. He and K.N. Fan, *Angew. Chem. Int. Ed.*, 2011, **50**, 7815 –7819.
24 A.M. Hengne, A.V. Malawadkar, N.S. Biradar and C.V. Rode, *RSC Adv.*, 2013, **4**, 9730-9736.
25 H. Heeres, R. Handana, D. Chunai, C. B. Rasrendra, B. Girisuta and H.J. Heeres, *Green Chem.*, 2009, **11**, 1247–1255.
26 A. Beloqui Redondo, D. Fodor, M.A. Brown, J.A. van Bokhoven, *Catal. Commun.*, 2014, **56**, 128–133.
27 P. Mars, J.J.F. Scholten, P. Zwietering, *Adv. Catal.*, 1963, **14**, 35–113.
28 S. Zhang, O. Metin, D. Su, S. Sun, *Angew. Chem. Int. Ed.*, 2013, **52**, 3681–3684.
29 N. Yi, H. Saltsburg and M. Flytzani-Stephanopoulos, *ChemSusChem*, 2013, **6**, 816–819.
30 D.A. Bulushev, S. Beloshapkin, P.E. Plyusnin, Y.V. Shubin, V.I. Bukhtiyarov, S.V. Korenev, J.H. Ross, *J. Catal.*, 2013, **299**, 171–180.
31 A. Ciftci, D.A.J.M. Ligthart, P. Pastorino, E.J.M. Hensen, *Appl. Catal. B: Environ.*, 2013, 130–131, 325–335.
32 S. Doniach and M. Sunjic, *J. Phys. C: Solid State Phys.*, 1970, **3(2)**, 285.
33 D.A. Shirley, *Phys. Rev. B*, 1972, **5**, 4709.
34 J.H. Scofield, *J. Electr. Spectrosc. Relat. Phenom.*, 1976, **8**, 129.
35 I. Kocemba Przem. Chem., 3 (82) 2003, 142.
36 A. Borodziński, M. Bonarowska *Langmuir* 1997, **13**, 5613
37 G. Kresse and J.Hafner, *Phys. Rev. B*, 1993, **47**, 558.
38 G. Kresse and J. Furthmuller, *Phys. Rev.B*, 1996, **54**, 11169.
39 J.P. Perdew, K. Burke and M. Ernzerhof, *Phys. Rev. Lett.*, 1996, **77**,3865.
40 P.E. Blochl, *Phys. Rev. B*, 1994, **50**, 17953.
41 G.Kresse and D.Joubert, *Phys. Rev. B*, 1999, **59**, 1758.
42 S. N. Steinmann, C. Corminboeuf, J. Chem. Phys., 2011, **13**, 044117.
43 S. N. Steinmann, C. Corminboeuf, *J. Chem. Theory Comput.*, 2011, **7**, 3567-3577.
44 K. Letchworth-Weaver and T.A. Arias, *Phys. Rev. B*, 2012, 86, 075140.
45 D. Gunceler, K. Letchworth-Weaver, R. Sundararaman, K.A. Schwarz and T.A. Arias, *Modelling and Simulation in Materials Science and Engineering*, 2013, **21**, 074005
46 P. Fleurat-Lessard, P. Dayal, A chemist view on reaction path determination, to be published. Available at http://perso.ens-lyon.fr/paul.fleurat-lessard/ReactionPath.html
47 G. Henkelman, B.P. Uberuaga and H. Jónsson, *J. Chem. Phys.*, 2000, **113**, 990
48 G. Henkelman and H. Jónsson, *J. Chem. Phys.*, 2000, **113**, 9978.
49 A. Heyden, A.T. Bell and F. J. Keil, *J. Chem. Phys.*, 2005,**123**, 224101.
50 N.K. Raman, T.L. Ward, C.J. Brinker, R. Sehgal, D.M. Smith, Z. Duan, M. Hampden-Smith, J.K. Bailey and T.J. Headley, *Appl. Catal., A: Gen.*, 1993, **69**, 65-82.
51 R.M. Mahfouz, M.R.H. Siddiqui, Sh.A. Al-Ahmari and W.Z. Alkayali, *Prog. React. Kinet. Mec.*, 2007 ,**32** , 1-27.
52 J.C. Calderon, G. Garcia, J.L. Rodriguez, M.J. Lazaro and E. Pastor, *Appl. Catal., B: Environ.*, 2015, **165**, 676-686.
53 Y. Zhou, G. Yang, H.-B. Pann C. Zhu, S. Fu, Q. Shi, D. Du, X. Cheng, J. Yang and C.M. Wai, *J. Mater. Chem. A*, 2015, **3**, 8459-8465.
54 M.Y. Chen, Y.-B. Huang, H. Pang, X.-X. Liu and Y. Fu, *Green Chem.*, 2015, **17**, 1710-1717.
55 J.S. Spendelow and A. Wieckowski, *Phys. Chem.-Chem. Phys.*, 2004, **6**, 5094-51188.
56 A. Lewera, W.P. Zhou, C. Vericat, J.H. Chung, R. Haasch, A. Wieckowski and P.S. Bagus, *Electrochem. Acta*, 2006, **51**, 3950-3956.
57 V. Mazzieri, F. Coloma-Pascual, A. Arcoya, P.C. L'Argentiere and N.S. Figoli, *Appl. Surf. Sci.*, 2003, **210**, 222-230.
58 A. Bossi, F. Garbassi, A. Orlandi, G. Petrini and L. Zanderighi, *Stud. Surf. Sci. Catal.*, 1979, **3**, 405.
59 P.G.J. Koopman, A.P.G. Kieboom and H. Van Bekkum, *J. Catal.*, 1981, **69**, 172–179.
60 A.M. Ruppert and T. Paryjczak Appl. *Catal. A: Gen.*, 2007, **320**, 80–90.
61 A. Guerrero-Ruiz, I. Rodriguez-Ramos and A. Arcoya, *Appl. Surf. Sci.*, 2013, **287**, 108– 116.
62 A. Guerrero-Ruiz, P. Badenes, I. Rodríguez-Ramos, E. Gallegos-Suarez and M. Pérez-Cadenas, *Appl. Catal., A: Gen.*, 1998, **173**, 313–321.
63 Q. Luo, T. Wang, M. Beller and H. Jiao, *J. Mol. Catal. A: Chem.*, 2013, **379**, 169-177.
64 A.H. Jeffrey, J. Scaranto, P. Ferrin, S. Li and M. Mavrikakis. *ACS Catal.*, 2014, **4**, 4434-4445.

Green Chemistry Accepted Manuscript

65 J.S. Yoo, F. Abild-Pedersen, J.K. Nørskov and F. Studt, *ACS Catal.*, 2014, **4**, 1226-1233.
66 Q. Luo, G. Fend, M. Beller, Matthias and H. Jiao, *J. Phys. Chem. C,* 2012, **116**, 4149-4156.
67 S.N. Steinmann, C. Michel, R. Schwiedernoch, J.-S. Filhol and P. Sautet, *ChemPhysChem*, 2015, **16**, 2307-2311.
68 J.A. Herron, J. Scaranto, P. Ferrin, S. Li and M. Mavrikakis, *ACS Catal.,* 2014, **4**, 4434-4445.
69 Y.K. Sun and W.H. Weinberg, *J. Chem. Phys.,* 1991, **94**, 4587-4599.
70 N.R. Avery, B.H. Tobi, A.B. Anton and W.H. Weinberg, *Surf. Sci.,* 1982, **122**, L574-L578.
71 B.H. Tobi, N.R. Avery, A.B. Anton and W.H. Weinberg, *J. Electron Spectrosc. Relat. Phenom.,* 1983, **29**, 317-321.
72 B. Meng, T.A. Jachimowski, Y. Sun and W.H. Weinberg, *Surf. Sci.,* 1994, **315**, L959-L963.
73 A.W. Grant, J.T. Ranney, C.T. Campbell, T. Evans and G. Thornton, *Catal. Lett.*, 2000, **65**, 159–168.
74 C.H. Bartholomew, in: Catalyst Deactivation, *Stud. Surf. Sci. Catal.*, Vol. 88, eds. B. Delmon and G.F. Froment (Elsevier, Amsterdam, 1994).

Green Chemistry Accepted Manuscript

This journal is © The Royal Society of Chemistry 20xx